

A shake and a surge: Assessing the possibility of an earthquake-triggered eruption at Steamboat Geyser


Mara H. Reed*¹, Anna Barth¹, Taka'aki Taira², Jamie Farrell³, and Michael Manga^{1,2}


5 ¹ Department of Earth and Planetary Science, University of California, Berkeley, Berkeley, USA


² Berkeley Seismological Lab, University of California, Berkeley, Berkeley, USA


³ Department of Geology and Geophysics, University of Utah, Salt Lake City, USA


* mhreed@berkeley.edu [corresponding author]

10  ORCID (Reed): 0000.0003.4185.2843

 ORCID (Barth): 0000.0002.8049.3276

 ORCID (Taira): 0000.0002.6170.797X

 ORCID (Farrell): 0000.0003.0620.6168

 ORCID (Manga): 0000.0003.3286.4682

15 **Keywords:** geyser, hydrothermal, eruption triggering, dynamic stress

Abstract

When and why earthquakes trigger the eruption of magma, mud, and water remain unclear. On 18 September 2022, Steamboat Geyser in Yellowstone, USA erupted 8.25 hours after a local M3.9 earthquake. The distribution
20 of Steamboat eruption intervals suggests a low probability of erupting so soon after the earthquake by chance. A seismometer 340 m from Steamboat recorded seismic waves with a peak ground velocity of 1.2 cm/s, which is the largest ground motion experienced in the area since at least March 2018 and is similar to values that have affected other Yellowstone geysers. Ambient seismic noise amplitude and relative seismic velocity changes in narrow frequency bands indicate a subsurface hydrothermal response. We find it likely that the eruption was
25 earthquake-triggered. If so, the hours-long delay suggests that dynamic strains from seismic waves caused changes in subsurface permeability and flow paths that enabled eruption.

1 Introduction

Stress changes produced by earthquakes affect the properties and flow of fluids in the crust. Earthquakes can promote the eruption of magmatic volcanoes (e.g., Linde and Sacks 1998; Walter et al. 2007; De la Cruz-Reyna et al. 2010; Bebbington and Marzocchi 2011) and mud volcanoes (e.g., Mellors et al. 2007; Bonini et al. 2016; Zhong et al. 2018), change the interval between geyser eruptions (Husen et al. 2004; Hurwitz et al. 2014), and modify the composition, pressure, and flow of groundwater (Wang and Manga 2021). The role of static stress changes and dynamic stresses from seismic waves, and what physical properties and processes change, remain the subject of active research (Seropian et al. 2021).

35

Steamboat Geyser at Norris Geyser Basin in Yellowstone National Park, USA has powerful major eruptions that reach heights in excess of 120 m. Most eruptions occur during active phases that last for months to years and are separated by periods of quiescence that last for years to decades (Reed et al. 2021). The most recent active phase began on 15 March 2018 and as of November 2023, there have been 167 major eruptions, the greatest number of eruptions in any known active phase. On 18 September 2022, Steamboat erupted after an interval of 90 d, the longest time between eruptions during the active phase thus far. The eruption began 8.25 h after a M3.9 earthquake with an epicenter 11 km from the geyser. Here we assess whether the eruption may have been triggered by the earthquake.

45 This paper is structured to emphasize a process of investigation that can be applied to other eruptions. First, we summarize the available data from Norris Geyser Basin and report on observations related to the earthquake and Steamboat's subsequent eruption. We then focus on different approaches to evaluating the possibility of earthquake-triggering. We first explore the probability of the eruption occurring on 18 September by chance and calculate the ground motions near Steamboat during the earthquake compared to those at other times in the active phase. We next search for evidence of other effects on the hydrothermal system by leveraging the available surface activity and seismic data. The final two sections are reserved for a discussion of this event in the context of other triggered eruptions and a summary of our findings.

50

2 Available data

55 Norris Geyser Basin [Figure 1] is well-monitored by sensors compared to other thermal areas in Yellowstone. Many permanent seismic stations are located throughout the Yellowstone area for earthquake monitoring,

providing a 1.5 magnitude of completeness (Farrell et al. 2009). Relevant to this study are two broadband seismometers located near Norris. Station YNM is situated within the geyser basin at ~340 m north of Steamboat while station YNR is located at ~2.19 km to the southeast. Both stations record significant anthropogenic noise during daylight hours. In addition to the seismometers, there are telemetered data from a streamgauge on Tantalus Creek through which 97% of Norris thermal discharge flows (Friedman 2007) and a network of nine temperature sensors placed in pools and runoff channels. Other non-telemetered temperature sensors are operated intermittently.

Major eruptions of Steamboat Geyser are detectable at one telemetered temperature sensor placed in one of Steamboat's runoff channels, the Tantalus Creek streamgauge, and both the YNM and YNR seismic stations. Because its eruptions are so spectacular, Steamboat is also tracked closely by geyser enthusiasts who submit eruption data and visual observations to the crowdsourced database GeyserTimes. A complete catalog of Steamboat eruptions exists for the recent active phase. Visual observations for most other Norris geysers are sporadic.

Whirligig Geyser, a small geyser ~580 m north of Steamboat, is the only other currently active feature at Norris with eruptions that are reliably detectable by a temperature sensor placed in a shared runoff channel for Whirligig and Constant Geysers. The two types of Whirligig eruptions are historically classified as *eruptions* and *minor eruptions/minors*. We will refer to the former as *major eruptions/majors* for clarity. Major eruptions discharge water out of three vents for several minutes and conclude when the pool almost fully drains; the much shorter minor eruptions are accompanied by lethargic splashing and end with a small drop in pool water level. All majors are detected when the sensor is operating but minors may be occasionally missed when they last <60 s, begin from a pool level below overflow, or occur at the same time as increased discharge from Constant. For calculating intervals, we only use GeyserTimes entries with an electronic (E) timecode, meaning the eruption start time was derived from temperature data.

80

3 Observations

Figure 2 provides an annotated overview of the data recorded on 18 September 2022 that show the timing of the earthquake and eruption signals from Steamboat and Whirligig Geysers. Temperature data for the combined runoff of Constant and Whirligig [Figure 2C] are shifted forward by 6 min to compensate for the approximate logger clock offset discerned from visual observations. Any time offset for Steamboat's temperature logger is unknown but likely small and irrelevant to our investigation because we do not analyze this data in detail.

85

3.1 Earthquake

The M_L 3.9 earthquake occurred at 6:55 local time (UTC-6) at a depth of 10.8 km (University of Utah Seismograph Stations 2022) and produced a peak ground velocity (PGV) of 1.2 cm/s at station YNM. To calculate this PGV, we
90 used three-component seismic data downloaded from the Incorporated Research Institutions for Seismology Data Management Center (IRIS DMC). We demeaned the data and removed the instrument response to obtain velocity records. Because YNM is a noisy station located by a popular trail, we applied a causal Butterworth bandpass filter between 0.8 and 30 Hz to reduce contributions from high-frequency anthropogenic and low-frequency ambient noise and then selected the maximum absolute amplitude of three-component ground motion.

95

This was the largest magnitude earthquake in the Grizzly Lake sequence, an intermittently active swarm that began in January 2022 and by the end of the year accumulated 1,177 events, >500 of which occurred during September (Yellowstone Volcano Observatory 2023). Swarms are sequences of earthquakes clustered in space and time that do not have a well-defined mainshock (Mogi 1963). In Yellowstone, they have been attributed to magmatic and/or
100 hydrothermal fluid migration (Waite and Smith 2002; Farrell et al. 2010; Shelly et al. 2013), and as many as half of earthquakes in the Yellowstone area occur as part of swarms (Farrell et al. 2009). Energy from the M3.9 earthquake can be seen on the spectrogram of the YNM vertical component in Figure 2A.

Runoff temperature data (a proxy for water discharge) suggest no immediate changes to Steamboat's minor
105 eruptions [Figure 2B] and an in-basin observer reported "nothing abnormal" after checking on the geyser at 7:16 (Wolf, 2022). There was no change to water level cycling at Constant (20–30 min period oscillation in Figure 2C) nor to cumulative discharge from Norris [Figure 2D]. The only possible indication of a reaction at Whirligig is the small temperature increase nearly concurrent with the earthquake. While not marked in the GeyserTimes database as an eruption, this signal bears similarities to minor eruptions confirmed by in-basin observers but not clearly
110 reflected in the temperature data (gold dash-dotted lines between 12:00 and 14:00 in Figure 2C). The potential minor eruption is notable because of its 47 min interval; major-to-minor intervals of <60 min are uncommon and could thus signify an earthquake response. However, due to the uncertainty in the logger clock offset and the challenges of discerning minor eruptions in the shared runoff channel, the possibility of a response from Whirligig is questionable.

115 **3.2 Major eruption of Steamboat Geyser**

Typical major eruptions at Steamboat start with a water jetting phase (duration usually <2 h) that builds to maximum height in the first few minutes and then subsides to heights below 60 m. Following this, the jet becomes more steam-dominated [Figure 3]. The eruption may later transition multiple times between water and steam phases until finally entering a low-energy steam phase that tapers to quiescence. Following each major eruption, the nearby
120 Cistern Spring will drain by several meters and then refill over several days (White et al. 1988; Wu et al. 2021).

On 18 September, an observer in the vicinity of Norris Geyser Basin heard the eruption begin at 15:10 and reported an initial water phase duration of ~ 10 min (Beverly 2022). We determine the volume of the water discharge pulse [Figure 2D] from the eruption by manually picking the start and end times, interpolating baseflow, and subtracting
125 baseflow volume from the total volume. This yields a volume of 373 m^3 ; however, wind speeds >1 m/s can decrease the water volume that enters Tantalus Creek and thus this should be considered a minimum estimate (Reed et al. 2021). In terms of both seismic spectral content and ejected water volume, the 18 September eruption was similar to other major eruptions (Reed et al. 2021; Reed and Manga 2023). Cistern Spring drained and refilled as normal. The major eruption's full duration of ~ 4 d was unusually long, but this may be related to the long prior interval. An
130 eruption on 25 August 2023 followed a 77.2 d interval and lasted at least 3.6 d (Beverly, 2023).

4 The case for a triggered eruption of Steamboat Geyser

When geysers have regular eruption intervals, identifying perturbations by earthquakes and other external influences is straightforward (Rinehart 1974; Husen et al. 2004; Hurwitz et al. 2014). Steamboat's eruptions were
135 somewhat regular during 2018–2020 when there was a small seasonal modulation of eruption intervals correlated with the hydrological cycle (Reed et al. 2021) and the average interval was 8 d. However, intervals have become more erratic and lengthened to an average of 26 d since 2021 [Figure 4A]. To build a case for earthquake-triggering of the 18 September eruption, we first focus on statistical modeling of the interval distribution and calculation of PGV for other earthquakes occurring since active phase initiation.

140 **4.1 Probability analysis**

What is the chance that the eruption coincidentally occurred on the day of the earthquake? For a very rough estimate, we can calculate the probability of Steamboat erupting on any given day in the active phase up to 18 September 2022 as the number of eruptions (156) divided by the number of days between then and 15 March 2018

(1648), which yields a probability of 10.6%. We can make a better probability estimate by considering the
145 distribution of eruption intervals. To do this, we fit a Weibull distribution function to the eruption intervals through
August 2023, excluding the interval for Steamboat's post-earthquake eruption [Figure 4B]. We then use this
distribution to calculate the probability of a 90 d eruption interval compared to intervals of 91–365 d. To estimate
uncertainty in the Weibull fitting parameters, we randomly resample the intervals 5000 times and follow the same
fitting and probability calculation procedure for each simulation [Figure 4C]. This results in a probability of 3.6%
150 with a 95% confidence interval of 2.8–5.2%.

4.2 History of peak ground velocity

How does the 1.2 cm/s PGV during the M3.9 earthquake compare to ground motions recorded during other
earthquakes? For the period of March 2018 through August 2023, we searched the Advanced National Seismic
System (ANSS) Comprehensive Catalog and identified 135 local earthquakes $\geq M2$ in a rectangular area bounded
155 by latitudes [44.603, 44.843] and longitudes [-110.873, -110.533], 12 regional earthquakes $\geq M5$ within a 1000 km
radius of Steamboat, and 751 teleseismic earthquakes $\geq M6$. At least one station was operating for 131 (97.0%) of
the local earthquakes, all 12 of the regional earthquakes, and 711 (94.7%) of the teleseismic earthquakes. Most of
the missed events occurred when YNM and YNR were both offline in January through April 2023, but it is unlikely
our analysis excludes any significant events. None of the missed local earthquakes during this period exceeded
160 M2.9 and none of the missed $\geq M7$ teleseismic earthquakes occurred within 5700 km.

We calculated PGV at both YNM and YNR by following the same procedure as before, using a causal Butterworth
bandpass filter between 0.8 and 30 Hz for the local earthquakes and 0.05 and 10 Hz for the regional and teleseismic
earthquakes. Instrument response correction can sometimes amplify unwanted noise at low frequencies (Havskov
165 and Alguacil 2016), so we used the comparatively less noisy YNR data to ground truth the YNM values. There
was significant (>1 order of magnitude) PGV disparity for 30 teleseismic events which we manually reviewed and
confirmed noise contamination at YNM.

Figure 5 shows the 119 local, 3 regional, and 47 teleseismic earthquakes exceeding a PGV of 10^{-2} cm/s. Values at
170 YNM were used unless the station was offline or noisy, in which case we substituted the PGV at YNR. The M3.9
earthquake is associated with the greatest PGV experienced at Norris Geyser Basin during Steamboat's recent
active phase. It is also the only event to exceed 1 cm/s, a threshold associated with earthquake responses at Old
Faithful and Daisy Geysers (Hurwitz et al. 2014). The next highest PGV of 0.8 cm/s is associated with a M7.6

175 earthquake in southwestern Mexico that occurred just one day later on 19 September. Of the next three highest
PGV events, only the M6.5 Stanley, Idaho earthquake occurred within close proximity (33.8 h prior) to a Steamboat
eruption, but the 8.3 d interval before this eruption was not anomalously short.

5 The case for other hydrothermal changes

180 So far, we have established the low probability that Steamboat erupted on the same day as the earthquake by
coincidence, and that the M3.9 earthquake produced the largest ground velocity at Norris Geyser Basin since the
ongoing active phase began in March 2018. Having exhausted what we can say about earthquakes and Steamboat's
eruptions in the context of the recent active phase, we now search for any evidence that the M3.9 earthquake
affected other parts of the Norris hydrothermal system.

5.1 Surface hydrothermal activity

185 Did other monitored thermal features react to the earthquake? In Section 3.1, we discussed the questionable minor
eruption at Whirligig immediately following the earthquake and the lack of change in thermal water discharge
through Tantalus Creek on 18 September. Now, we explore Whirligig's activity and Tantalus Creek discharge for
the period of August through October 2022 to assess long-term trends [Figure 6]. We use eruptions in the
GeyserTimes catalog to calculate three different measures of Whirligig's activity. First, we separate the data into
190 daily slices and determine both the mean interval prior to detected eruptions and the fraction of minor eruptions for
each day. Because some minors go undetected, these measures may be longer than and lower than the actual values,
respectively. We finally calculate major-to-major eruption intervals. Tantalus Creek data is presented without
further processing.

195 Over this three-month period, the daily fraction of minor eruptions at Whirligig increases to reach >0.85 in all of
October. The daily mean interval becomes less variable between mid-September and 10 October before returning
to the same length and variability seen in August. Major-to-major intervals are generally consistent with a slight
increasing trend through September, becoming more variable in mid-September with a steeper increasing trend.
None of these changes appear tied to the M3.9 earthquake on 18 September.

200

The Tantalus Creek hydrograph shows a slight upward trend through the selected time period which does not
change following the earthquake. At shorter timescales, there are sharp discharge peaks associated with rainfall

events except for the spike on 18 September which is caused by runoff from Steamboat's eruption [Figure 2D]. The drop in discharge on 19 September is most likely due to the diurnal signal arising from increased evaporation during warm daytime hours (Clor et al. 2007). Thus, we again find no support for an earthquake response in the overall thermal discharge from Norris.

5.2 Ambient seismic noise amplitude

Were there any changes to the strength of ambient seismic noise? Hydrothermal areas generate tremor that has been primarily attributed to bubble collapse and nucleation (e.g., Kedar et al. 1998; Legaz et al. 2009; Vandemeulebrouck et al. 2014; Nayak et al. 2020; Liu et al. 2023). Very little has been published about hydrothermal tremor at Norris Geyser Basin since Iyer and Hitchcock (1974) identified the area as a source of seismic noise. Dawson et al. (2012) identified localized, >15 Hz impulses occurring 1–2 times per second and continuous 8 Hz tremor in the southern half of Norris Geyser Basin during a 2003 broadband seismometer campaign. Wu et al. (2021) found continuous 1–5 Hz tremor at Steamboat Geyser and Cistern Spring that varied in space and amplitude over Steamboat's eruptive cycle. While station YNM is likely too far away to detect tremor sources local to Steamboat during non-eruptive periods, we can still explore the relative power of any hydrothermal tremor local to the station. Here, we narrow our attention to the earthquake-triggering assessment at hand and leave a detailed characterization of time-varying spectral content at this station for future study.

Seismic spectral amplitude measurements (SSAM) are a computationally inexpensive way to represent relative signal strength in different frequency bands over time (Rogers and Stephens 1995). We compute SSAM for narrow 1 Hz bands between 0.5 to 5.5 Hz, a range chosen to match low frequency tremor observed in Yellowstone thermal areas (Wu et al. 2019, 2021; Liu et al. 2023) and to avoid contamination from Steamboat's broadband (5–45 Hz) eruption signal (Reed and Manga, 2023). After selecting the raw, vertical-component seismic data for overnight hours (20:30–6:30) during August–October 2022, we remove instrument response to obtain velocity, slice the data into 1 h segments, and apply acausal, 4 corner Butterworth bandpass filters to match the bands of interest. We then calculate SSAM as the median of the absolute valued velocity in each segment.

Only the 0.5–1.5 Hz SSAM show a response to the earthquake [Figure 7]. In this band, SSAM generally increase up until the M3.9 earthquake, after which there is a downward step change. There is also a cyclic increase in SSAM that occurs every 10–12 d; this period does not change following the earthquake. We compute spectrograms of the unfiltered vertical seismic velocity data for one of the periodic SSAM increases beginning 20 August and the step

change on 18 September. In both cases, the dominant signal in the 0.5–1.5 Hz range is centered just below 1 Hz. This signal decreases in frequency and increases in power at the onset of the periodic SSAM fluctuation; it increases
235 in frequency and decreases in power after the earthquake. We note that significant decreases in SSAM are not unique to the M3.9 event and have occurred multiple times prior to and during Steamboat’s active phase (Reed et al., 2021). However, because the 0.5–1.5 Hz tremor weakened almost immediately following the earthquake and was accompanied by other sudden shifts in high frequency signals (>27 Hz in Figure 2A), we argue the changes in 0.5–1.5 Hz tremor can reasonably be attributed to processes triggered by the earthquake.

240 **5.3 Relative seismic velocity changes**

Were there changes to subsurface properties? Local earthquakes are thought to decrease seismic velocity in hydrothermal areas by clearing fractures during pore pressure fluctuations (e.g., Brodsky et al. 2003; Manga et al. 2012). We can apply ambient noise seismic interferometry (e.g., Brenguier et al. 2008; Snieder and Larose 2013) using the three-component YNM data to obtain relative seismic velocity changes (dv/v) of subsurface media. We
245 focus our analysis on the month of September 2022 and compute noise cross-correlation functions (NCFs) in four different frequency bands (0.5–1.5, 1.5–2.5, 2.5–3.5, and 3.5–4.5 Hz) using MSNoise (Lecocq et al., 2014).

Our data processing methods are similar to those described in Brenguier et al. (2008) and Taira et al. (2018). First, we correct instrument response on 24 h continuous data slices to obtain ground displacement and apply a bandpass
250 filter between 0.08 and 8.0 Hz. Daily bandpass-filtered recordings are then down-sampled from 100 to 20 Hz and split into 30 min sections. Following Hobiger et al. (2014), we compute NCFs for cross-component pairs (i.e., vertical-north, vertical-east, and north-east) where a spectral whitening process can be applied to minimize signals associated with local and teleseismic earthquakes. Subsequently, one-bit normalization is applied at the frequency bands of interest.

255

We measure temporal change in dv/v through the time delay estimate (dt) for a pair of NCFs with the moving window cross-spectral technique (Clarke et al. 2011), assuming a homogeneous velocity where

$$\frac{dv}{v} = -\frac{dt}{t}. \quad (1)$$

We only use dt in a moving window where the value of cross-correlation between the stacked and reference NCFs
260 exceeds 0.85. The windows overlap by 50% and the window lengths are equivalent to the longest period in each frequency band used. Our analysis focuses on a 3 s coda of NCFs (–5 to –2 s and 2 to 5 s) to measure time delays

between the 60, 120, 240, and 360 min stacks of NCFs and reference NCFs computed for data between December 2021 and December 2022.

265 A sudden dv/v reduction of $\sim 3 \pm 1\%$ following the M3.9 earthquake appears in the 1.5–2.5 Hz frequency band
when using 60 and 120 min stacking [Figure 8A]. The decrease in dv/v for the 1.5–2.5 Hz band is not present in
the 240 and 360 min stacking results, which supports prompt recovery of seismic velocity. Though the uncertainties
are large and there are other sudden, unexplained variations in dv/v up to 1.5% for this band in September, the
timing and magnitude of the $\sim 3\%$ velocity reduction are significant. Our analysis did not find sudden dv/v changes
270 after the earthquake in the 0.5–1.5, 2.5–3.5, and 3.5–4.5 Hz bands for any of our stacking methods. This suggests
the change in seismic velocity occurred at a narrow depth interval. Assuming a ratio of P-wave to S-wave velocity
(v_p/v_s) of 1.6 (Husen et al. 2004) and that the coda of our NCFs is dominated by Rayleigh waves, we calculate a
surface wave sensitivity kernel with a 1D P-wave velocity model used by the University of Utah Seismograph
Stations to determine earthquake locations [Figure 8B–C]. We find that the reduction in relative seismic velocity
275 likely occurred at a depth of 300–500 m given the lack of dv/v changes in frequency bands other than 1.5–2.5 Hz.

6 Discussion

Overall, we find it plausible that Steamboat’s major eruption on 18 September 2022 was earthquake-triggered. The
low probability of eruption on that day compared to days in the following months is encouraging but does not prove
280 the eruption was related to the earthquake. Our best evidence comes from the PGV results; we established that the
M3.9 earthquake produced a PGV of 1.2 cm/s and that no other analyzed earthquake produced ground motions >1
cm/s since the active phase began. The immediate post-earthquake reductions in SSAM and dv/v indicate changes
in subsurface properties and shed light on a triggering mechanism.

285 Previous studies that documented temporary decreases of dv/v following local and teleseismic earthquakes in
volcanic (e.g., Lesage et al. 2014; Brenguier et al. 2014; Nimiya et al. 2017) and hydrothermal systems (e.g., Taira
and Brenguier 2016; Taira et al. 2018; Saade et al. 2019) have attributed the drop in seismic velocity to the opening
of cracks. The relationship between peak dynamic stress, PDS , and peak ground velocity is

$$PDS = G \frac{PGV}{v_s} \quad (2)$$

290 where G is the shear modulus (Hill et al. 1993; van der Elst and Brodsky 2010). Using representative values of
 $G=13$ GPa and $v_s=2.3$ km/s for water-saturated silica sinter (Munoz-Saez et al. 2016), the M3.9 earthquake

generated a peak dynamic stress of ~ 0.07 MPa. While larger than those from solid Earth tides and barometric pressure changes, this stress is likely too low to promote new fracture formation. The quick recovery of dv/v (hours vs. weeks to months in the cited studies) further implies that there were no permanent changes in rock properties. 295 Instead, the decrease in velocity may result from an increase in gas fraction or decrease in water levels which would raise the bulk rock compressibility.

There are physical and thermal mechanisms that enable earthquakes to trigger eruptions without the need for new fractures. Simply disturbing the pool of some thermal features can trigger boiling or eruptions; historically, tourists 300 sometimes induced eruptions by throwing soap (e.g., Hague 1889; Graham 1893) or objects (e.g., Allen and Day 1935) into geysers. Vibrations have also been shown to trigger bubble nucleation and eruption in laboratory geysers (Steinberg et al. 1982). In these examples, the water must be superheated or primed to erupt so that nucleating bubbles or promoting convection is sufficient to initiate an eruption (Rinehart 1974). However, the 8.25 h delay between earthquake and eruption at Steamboat is too long to favor these mechanisms. There are other examples 305 where changes to geysers occur gradually. After the 2002 M7.9 Denali earthquake, Daisy Geyser's activity decreased from variable 2.3–3.5 h eruption intervals to consistent 1.5–1.7 h intervals over a 24 h period (Husen et al. 2004; Hurwitz et al 2014). The recovery to its pre-earthquake state occurred more gradually over several months. This is in line with some other hydrogeological responses in groundwater levels (e.g., Brodsky et al. 2003; Roeloffs et al. 2003; Shi et al. 2015) and streamflow (e.g., Muir-Wood and King 1993; Manga 2001; Wang and Manga 310 2015) that take days to weeks to reach their peak and then recover to pre-earthquake conditions over months.

Daisy's 2002 earthquake response and our proposed triggering of Steamboat would be best explained by earthquake-induced changes in hydraulic head or subsurface permeability (Ingebritsen and Rojstaczer 1996) that affect fluid and heat flow. Existing fractures just north of Steamboat, identified from geologic mapping and airborne 315 infrared surveys, trend roughly toward YNM (White et al. 1988; Jaworowski et al. 2006). If the earthquake affected subsurface permeability, the decrease in relative seismic velocity could represent fluid and thus heat flow away from a 300–500 m deep reservoir, perhaps toward Steamboat along these fractures. The persistent, ~ 1 Hz tremor band identified from SSAM could be interpreted as resonance of or boiling within a separate fluid-filled conduit or cavity. If boiling decreased and/or the fluid level dropped, this might explain the observed increase in resonant 320 frequency (Rudolph et al. 2018; Teshima et al. 2022). The increased distance between YNM and the fluid-filled part of the conduit and/or the reduction in boiling would then explain the weakening tremor.

The reasons for why geysers react to some earthquakes but not others remain elusive. We restricted our PGV analysis to earthquakes during Steamboat's active phase, but Norris Geyser Basin has experienced greater dynamic stresses from local and regional earthquakes prior to March 2018. Most recently, a local M_w 4.8 earthquake produced a PGV of >3 cm/s at YNM in 2014 but did not trigger an eruption (Reed et al. 2021). Nor were major eruptions recorded following any of five $\geq M5$ earthquakes that occurred within 15 km of Norris in 1975 and 1976. (For completeness, we note there exists an unconfirmed logbook report of steam phase behavior at Steamboat two days after the 30 June 1975 Yellowstone National Park earthquake (Bellingham 2023), but we choose to discount it because it is not referenced in the more authoritative records from that year.) Even the 1959 M_w 7.2 Hebgen Lake earthquake, which triggered eruptions in dormant geysers and springs with no known eruptive history across Yellowstone and increased turbidity in Norris thermal features (White et al. 1988), failed to elicit an eruption of Steamboat. The more distant 1983 M_w 6.9 Borah Peak earthquake also affected geyser activity in a localized area of the Upper Geyser Basin (Hutchinson 1985), but we found no records of effects at Norris and again, there was no reported Steamboat eruption.

Studies of volcanic eruptions indicate that the internal state of a volcano is a primary control on whether or not an earthquake-triggered eruption occurs (e.g., Bebbington and Marzocchi 2011; Sawi and Manga 2018; Fariás and Basualto 2020). This is likely true of geysers as well. None of the earthquakes mentioned above except for the Borah Peak earthquake coincided with Steamboat active phases, and we speculate that earthquake-triggering might only be possible at Steamboat when the local system is capable of frequent major eruptions. Steamboat erupted just 6 more times in 13 months following the Borah Peak earthquake before reentering dormancy; a lack of response to that event might imply that the Steamboat system was already headed toward dormancy at the time.

7 Conclusion

On 18 September 2022, Steamboat Geyser erupted just 8.25 h after a nearby $M3.9$ earthquake. We conclude it is more likely than not that this eruption was triggered by the earthquake for the following reasons:

1. There is a low probability that the eruption occurred on the day of the earthquake by chance based on Weibull modeling of the eruption interval population.
2. The 1.2 cm/s PGV recorded at YNM is the greatest experienced at Norris Geyser Basin during Steamboat's recent active phase. It also exceeds a threshold (1 cm/s) associated with earthquake-related responses at other geysers, mud volcanoes, and streams.

3. Seismic data suggest possible subsurface hydrothermal changes following the earthquake, supporting the feasibility of a response from Steamboat. While the surface discharge of monitored Norris thermal features did not change, our SSAM results suggest a weakening or deepening of a 0.5–1.5 Hz tremor source and our dv/v results indicate a short-lived velocity reduction in material at 300–500 m depth.

However, we keep in mind these corresponding caveats:

1. Low chance of coincidence does not mean a coincidence is impossible. The 90 d interval before this eruption is an outlier in the ongoing active phase which makes an interval distribution-based probability analysis somewhat less compelling.
2. There are no historical reports of Steamboat Geyser having major eruptions following other energetic local or regional earthquakes. It is possible that earthquake-triggering can only occur at Steamboat during active phases; however, the 1983 M6.9 Borah Peak earthquake failed to trigger an eruption during Steamboat's 1980s active phase despite affecting other Yellowstone geysers.
3. More work is needed to understand the source mechanism of the 0.5–1.5 Hz tremor and how changes in frequency and amplitude may relate to an eruption triggering mechanism. Additionally, probing relative seismic velocity changes at such short timescales is difficult as less noise can be removed via stacking. The dv/v reduction we found was not much larger than background variations.

Finally, this analysis was only possible due to the number of monitoring instruments at Norris Geyser Basin. The installation of more seismometers and eruption recording equipment in hydrothermal areas would increase the chance of identifying earthquake-triggered eruptions when they occur and documenting the accompanying subsurface changes.

Author contributions

MHR: Conceptualization, Formal analysis (PGV, eruption interval, eruption volume, and SSAM calculations), Writing - Original Draft, Writing - Review & Editing, Visualization

AB: Conceptualization, Formal analysis (Weibull modeling), Writing - Original Draft, Writing - Review & Editing, Visualization

TT: Formal analysis (dv/v and sensitivity kernel), Writing - Original Draft, Writing - Review & Editing, Visualization

JF: Resources (1D velocity model), Writing - Review & Editing

MM: Conceptualization, Writing - Original Draft, Writing - Review & Editing

385

Acknowledgements

We thank Graham Meech for the wonderful photo of Steamboat and MA Bellingham for her assistance in assessing the quality of Whirligig data. We also thank the University of Utah for maintaining seismometers in Yellowstone. Financial support for this work came from NSF Grant EAR2116573, the Northern California Chapter of the ARCS
390 Foundation, the Miller Institute for Basic Research in Science, and CIFAR Earth 4D.

Data availability

GeyserTimes data are available via <https://geysertimes.org/retrieve.php>. The Yellowstone Seismic Network (network code WY) is operated by the University of Utah Seismograph Stations and seismic data are made available
395 through the EarthScope Consortium's IRIS DMC (<https://ds.iris.edu/ds/nodes/dmc/>). Earthquake data come from the ANSS Comprehensive Catalog published by the U.S. Geological Survey (<https://earthquake.usgs.gov/data/comcat/>). The Tantalus Creek streamgage is operated jointly by the U.S. Geological Survey and the U.S. National Park Service; discharge data is available at <https://waterdata.usgs.gov/monitoring-location/06036940>. Telemetered temperature sensors are maintained by the
400 Yellowstone Volcano Observatory and the raw data used in this study are attached in the Supplementary Material.

References

- Allen, E. T., & Day, A. L. (1935). *Hot springs of the Yellowstone National Park*. Carnegie Institution of Washington. URL: <https://catalog.hathitrust.org/Record/001639423>
405
- Bebbington, M. S., & Marzocchi, W. (2011). Stochastic models for earthquake triggering of volcanic eruptions. *Journal of Geophysical Research: Solid Earth*, 116(B5). DOI: [10.1029/2010JB008114](https://doi.org/10.1029/2010JB008114)
- Bellingham, M. (2023). *Note ID 32609* [database entry; transcription of entry in the 1975 Norris Geyser Basin
410 logbook]. GeyserTimes. URL: <https://geysertimes.org/note.php?id=32609>

Beverly, C. (2022). *Eruption ID 1384597* [database entry]. GeyserTimes. URL: <https://geysertimes.org/eruption.php?id=1384597>

415 Beverly, C. (2023). *Note ID 27844* [database entry]. GeyserTimes. URL: <https://geysertimes.org/note.php?id=27844>

Bonini, M., Rudolph, M. L., & Manga, M. (2016). Long- and short-term triggering and modulation of mud volcano eruptions by earthquakes. *Tectonophysics*, 672–673, 190–211. DOI: [10.1016/j.tecto.2016.01.037](https://doi.org/10.1016/j.tecto.2016.01.037)

420

Brenguier, F., Campillo, M., Takeda, T., Aoki, Y., Shapiro, N. M., Briand, X., Emoto, K., & Miyake, H. (2014). Mapping pressurized volcanic fluids from induced crustal seismic velocity drops. *Science*, 345(6192), 80–82. DOI: [10.1126/science.1254073](https://doi.org/10.1126/science.1254073)

425 Brenguier, F., Shapiro, N. M., Campillo, M., Ferrazzini, V., Duputel, Z., Coutant, O., & Nercessian, A. (2008). Towards forecasting volcanic eruptions using seismic noise. *Nature Geoscience*, 1(2), 126–130. DOI: [10.1038/ngeo104](https://doi.org/10.1038/ngeo104)

430 Brodsky, E. E., Roeloffs, E., Woodcock, D., Gall, I., & Manga, M. (2003). A mechanism for sustained groundwater pressure changes induced by distant earthquakes. *Journal of Geophysical Research: Solid Earth*, 108(B8). DOI: [10.1029/2002JB002321](https://doi.org/10.1029/2002JB002321)

435 Clarke, D., Zaccarelli, L., Shapiro, N. M., & Brenguier, F. (2011). Assessment of resolution and accuracy of the moving window cross spectral technique for monitoring crustal temporal variations using ambient seismic noise. *Geophysical Journal International*, 186(2), 867–882. DOI: [10.1111/j.1365-246X.2011.05074.x](https://doi.org/10.1111/j.1365-246X.2011.05074.x)

Clor, L. E., Lowenstern, J. B., & Heasler, H. P. (2007). *Systematics of Water Temperature and Flow at Tantalus Creek During Calendar Year 2005, Norris Geyser Basin, Yellowstone National Park, Wyoming* (Scientific Investigations Report 2007–5234). U.S. Geological Survey. DOI: [10.3133/sir20075234](https://doi.org/10.3133/sir20075234)

440

- Dawson, P. B., Benítez, M. C., Lowenstern, J. B., & Chouet, B. A. (2012). Identifying bubble collapse in a hydrothermal system using hidden Markov models. *Geophysical Research Letters*, 39(1). DOI: [10.1029/2011GL049901](https://doi.org/10.1029/2011GL049901)
- 445 De la Cruz-Reyna, S., Tárraga, M., Ortiz, R., & Martínez-Bringas, A. (2010). Tectonic earthquakes triggering volcanic seismicity and eruptions. Case studies at Tungurahua and Popocatépetl volcanoes. *Journal of Volcanology and Geothermal Research*, 193(1), 37–48. DOI: [10.1016/j.jvolgeores.2010.03.005](https://doi.org/10.1016/j.jvolgeores.2010.03.005)
- Fariás, C., & Basualto, D. (2020). Reactivating and calming volcanoes: The 2015 MW 8.3 Illapel megathrust strike. 450 *Geophysical Research Letters*, 47(16), e2020GL087738. DOI: [10.1029/2020GL087738](https://doi.org/10.1029/2020GL087738)
- Farrell, J., Husen, S., & Smith, R. B. (2009). Earthquake swarm and b-value characterization of the Yellowstone volcano-tectonic system. *Journal of Volcanology and Geothermal Research*, 188(1), 260–276. DOI: [10.1016/j.jvolgeores.2009.08.008](https://doi.org/10.1016/j.jvolgeores.2009.08.008)
- 455 Farrell, J., Smith, R. B., Taira, T., Chang, W.-L., & Puskas, C. M. (2010). Dynamics and rapid migration of the energetic 2008–2009 Yellowstone Lake earthquake swarm. *Geophysical Research Letters*, 37(19). DOI: [10.1029/2010GL044605](https://doi.org/10.1029/2010GL044605)
- 460 Friedman, I. (2007). *Monitoring changes in geothermal activity at Norris Geysir Basin by satellite telemetry, Yellowstone National Park, Wyoming*. In L. A. Morgan (Ed.), *Integrated geoscience studies in the Greater Yellowstone Area—Volcanic, tectonic, and hydrothermal processes in the Yellowstone geocosystem* (Professional Paper 1717, pp. 509–532). U.S. Geological Survey. DOI: [10.3133/pp1717](https://doi.org/10.3133/pp1717)
- 465 Graham, J. C. (1893). Some experiments with an artificial geyser. *American Journal of Science*, 55(265–270), 54–60. URL: <https://www.proquest.com/docview/89599353>
- Hague, A. (1889). Soaping geysers. *Science*, 13(328), 382–384. DOI: [10.1126/science.ns-13.328.382.b](https://doi.org/10.1126/science.ns-13.328.382.b)
- 470 Havskov, J., & Alguacil, G. (2016). Correction for instrument response. In *Instrumentation in earthquake seismology* (pp. 197–230). Springer International Publishing. DOI: [10.1007/978-3-319-21314-9_6](https://doi.org/10.1007/978-3-319-21314-9_6)

- Hill, D. P., Reasenber, P. A., Michael, A., Arabaz, W. J., G. Beroza, Brumbaugh, D., Brune, J. N., Castro, R., Davis, S., Depolo, D., Ellsworth, W. L., Gomberg, J., Harmsen, S., House, L.,
475 Jackson, S. M., Johnston, M. J. S., Jones, L., Keller, R., Malone, S., ... Zollweg, J. (1993). Seismicity remotely triggered by the magnitude 7.3 Landers, California, earthquake. *Science* 260(5114), 1617–1623. DOI: [10.1126/science.260.5114.1617](https://doi.org/10.1126/science.260.5114.1617)
- Hobiger, M., Wegler, U., Shiomi, K., & Nakahara, H. (2014). Single-station cross-correlation analysis of ambient
480 seismic noise: Application to stations in the surroundings of the 2008 Iwate-Miyagi Nairiku earthquake. *Geophysical Journal International*, 198(1), 90–109. DOI: [10.1093/gji/ggu115](https://doi.org/10.1093/gji/ggu115)
- Hurwitz, S., Sohn, R. A., Luttrell, K., & Manga, M. (2014). Triggering and modulation of geyser eruptions in
485 Yellowstone National Park by earthquakes, earth tides, and weather. *Journal of Geophysical Research: Solid Earth*, 119(3), 1718–1737. DOI: [10.1002/2013JB010803](https://doi.org/10.1002/2013JB010803)
- Husen, S., Taylor, R., Smith, R. B., & Healsen, H. (2004). Changes in geyser eruption behavior and remotely
490 triggered seismicity in Yellowstone National Park produced by the 2002 M 7.9 Denali fault earthquake, Alaska. *Geology*, 32(6), 537–540. DOI: [10.1130/G20381.1](https://doi.org/10.1130/G20381.1)
- Hutchinson, R. A. (1985). *Hydrothermal changes in the Upper Geyser Basin, Yellowstone National Park, after the 1983 Borah Peak, Idaho, earthquake*. In R. S. Stein & R. C. Bucknam (Eds.), *Proceedings of workshop XXVIII on the Borah Peak, Idaho earthquake* (Open-File Report 85-290-A, pp. 612–624). U.S. Geological Survey. DOI: [10.3133/ofr85290A](https://doi.org/10.3133/ofr85290A)
- 495 Ingebritsen, S. E., & Rojstaczer, S. A. (1996). Geyser periodicity and the response of geysers to deformation. *Journal of Geophysical Research: Solid Earth*, 101(B10), 21891–21905. DOI: [10.1029/96JB02285](https://doi.org/10.1029/96JB02285)
- Iyer, H. M., & Hitchcock, T. (1974). Seismic noise measurements in Yellowstone National Park. *Geophysics*, 39(4),
500 389–400. DOI: [10.1190/1.1440437](https://doi.org/10.1190/1.1440437)

Jaworowski, C., Heasler, H. P., Hardy, C. C., & Queen, L. P. (2006). Control of hydrothermal fluids by natural fractures at Norris Geyser Basin. *Yellowstone Science*, 14(4), 13–23. URL: https://www.volcano.gov/vsc/file_mgr/file-25/JaworowskiYellSciFall06.pdf

505

Kedar, S., Kanamori, H., & Sturtevant, B. (1998). Bubble collapse as the source of tremor at Old Faithful Geyser. *Journal of Geophysical Research: Solid Earth*, 103(B10), 24283–24299. DOI: [10.1029/98JB01824](https://doi.org/10.1029/98JB01824)

510

Lecocq, T., Caudron, C., & Brenguier, F. (2014). MSNoise, a Python package for monitoring seismic velocity changes using ambient seismic noise. *Seismological Research Letters*, 85(3), 715–726. DOI: [10.1785/0220130073](https://doi.org/10.1785/0220130073)

515

Legaz, A., Revil, A., Roux, P., Vandemeulebrouck, J., Gouédard, P., Hurst, T., & Bolève, A. (2009). Self-potential and passive seismic monitoring of hydrothermal activity: A case study at Iodine Pool, Waimangu geothermal valley, New Zealand. *Journal of Volcanology and Geothermal Research*, 179(1), 11–18. DOI: [10.1016/j.jvolgeores.2008.09.015](https://doi.org/10.1016/j.jvolgeores.2008.09.015)

520

Lesage, P., Reyes-Dávila, G., & Arámbula-Mendoza, R. (2014). Large tectonic earthquakes induce sharp temporary decreases in seismic velocity in Volcán de Colima, Mexico. *Journal of Geophysical Research: Solid Earth*, 119(5), 4360–4376. DOI: [10.1002/2013JB010884](https://doi.org/10.1002/2013JB010884)

525

Linde, A. T., & Sacks, I. S. (1998). Triggering of volcanic eruptions. *Nature*, 395, 888–890. DOI: [10.1038/27650](https://doi.org/10.1038/27650)

Liu, C.-N., Lin, F.-C., Manga, M., Farrell, J., Wu, S.-M., Reed, M. H., Barth, A., Hungerford, J., & White, E. (2023). Thumping cycle variations of Doublet Pool in Yellowstone National Park, USA. *Geophysical Research Letters*, 50(4), e2022GL101175. DOI: [10.1029/2022GL101175](https://doi.org/10.1029/2022GL101175)

Manga, M. (2001). Origin of postseismic streamflow changes inferred from baseflow recession and magnitude-distance relations. *Geophysical Research Letters*, 28(10), 2133–2136. DOI: [10.1029/2000GL012481](https://doi.org/10.1029/2000GL012481)

530

Manga, M., Beresnev, I., Brodsky, E. E., Elkhoury, J. E., Elsworth, D., Ingebritsen, S. E., Mays, D. C., & Wang, C.-Y. (2012). Changes in permeability caused by transient stresses: Field observations, experiments, and mechanisms. *Reviews of Geophysics*, 50(2). DOI: [10.1029/2011RG000382](https://doi.org/10.1029/2011RG000382)

Mellors, R., Kilb, D., Aliyev, A., Gasanov, A., & Yetirmishli, G. (2007). Correlations between earthquakes and
535 large mud volcano eruptions. *Journal of Geophysical Research: Solid Earth*, 112(B4). DOI:
[10.1029/2006JB004489](https://doi.org/10.1029/2006JB004489)

Mogi, K. (1963). Some discussions on aftershocks, foreshocks and earthquake swarms—The fracture of a semi
540 finite body caused by an inner stress origin and its relation to the earthquake phenomena. *Bulletin of the Earthquake
Research Institute*, 41, 615–658.

Muir-Wood, R., & King, G. C. P. (1993). Hydrological signatures of earthquake strain. *Journal of Geophysical
Research: Solid Earth*, 98(B12), 22035–22068. DOI: [10.1029/93JB02219](https://doi.org/10.1029/93JB02219)

545 Munoz-Saez, C., Saltiel, S., Manga, M., Nguyen, C., & Gonnermann, H. (2016). Physical and hydraulic properties
of modern sinter deposits: El Tatio, Atacama. *Journal of Volcanology and Geothermal Research*, 325, 156–168.
DOI: [10.1016/j.jvolgeores.2016.06.026](https://doi.org/10.1016/j.jvolgeores.2016.06.026)

Nayak, A., Manga, M., Hurwitz, S., Namiki, A., & Dawson, P. B. (2020). Origin and properties of hydrothermal
550 tremor at Lone Star Geyser, Yellowstone National Park, USA. *Journal of Geophysical Research: Solid Earth*,
125(12), e2020JB019711. DOI: [10.1029/2020JB019711](https://doi.org/10.1029/2020JB019711)

Nimiya, H., Ikeda, T., & Tsuji, T. (2017). Spatial and temporal seismic velocity changes on Kyushu Island during
555 the 2016 Kumamoto earthquake. *Science Advances*, 3(11), e1700813. DOI: [10.1126/sciadv.1700813](https://doi.org/10.1126/sciadv.1700813)

Reed, M. H., & Manga, M. (2023). Snow suppresses seismic signals from Steamboat Geyser. *Geophysical
Research Letters*, 50(12), e2023GL103904. DOI: [10.1029/2023GL103904](https://doi.org/10.1029/2023GL103904)

Reed, M. H., Munoz-Saez, C., Hajimirza, S., Wu, S.-M., Barth, A., Girona, T., Rasht-Behesht, M., White, E. B.,
560 Karplus, M. S., Hurwitz, S., & Manga, M. (2021). The 2018 reawakening and eruption dynamics of Steamboat
Geyser, the world's tallest active geyser. *Proceedings of the National Academy of Sciences*, 118(2). DOI:
[10.1073/pnas.2020943118](https://doi.org/10.1073/pnas.2020943118)

Rinehart, J. S. (1974). Geysers. *Eos*, 55(12), 1052–1062. DOI: [10.1029/EO055i012p01052](https://doi.org/10.1029/EO055i012p01052)

565

Roeloffs, E., Sneed, M., Galloway, D. L., Sorey, M. L., Farrar, C. D., Howle, J. F., & Hughes, J. (2003). Water-level changes induced by local and distant earthquakes at Long Valley caldera, California. *Journal of Volcanology and Geothermal Research*, 127(3), 269–303. DOI: [10.1016/S0377-0273\(03\)00173-2](https://doi.org/10.1016/S0377-0273(03)00173-2)

570 Rogers, J. A., & Stephens, C. D. (1995). SSAM: Real-time seismic spectral amplitude measurement on a PC and its application to volcano monitoring. *Bulletin of the Seismological Society of America*, 85(2), 632–639. DOI: [10.1785/BSSA0850020632](https://doi.org/10.1785/BSSA0850020632)

Rudolph, M. L., Sohn, R. A., & Lev, E. (2018). Fluid oscillations in a laboratory geyser with a bubble trap. *Journal of Volcanology and Geothermal Research*, 368, 100–110. DOI: [10.1016/j.jvolgeores.2018.11.003](https://doi.org/10.1016/j.jvolgeores.2018.11.003)

575

Saade, M., Araragi, K., Montagner, J. P., Kaminski, E., Roux, P., Aoki, Y., & Brenguier, F. (2019). Evidence of reactivation of a hydrothermal system from seismic anisotropy changes. *Nature Communications*, 10, 5278. DOI: [10.1038/s41467-019-13156-8](https://doi.org/10.1038/s41467-019-13156-8)

580

Sawi, T. M., & Manga, M. (2018). Revisiting short-term earthquake triggered volcanism. *Bulletin of Volcanology*, 80(57). DOI: [10.1007/s00445-018-1232-2](https://doi.org/10.1007/s00445-018-1232-2)

Seropian, G., Kennedy, B. M., Walter, T. R., Ichihara, M., & Jolly, A. D. (2021). A review framework of how earthquakes trigger volcanic eruptions. *Nature Communications*, 12, 1004. DOI: [10.1038/s41467-021-21166-8](https://doi.org/10.1038/s41467-021-21166-8)

585

Shelly, D. R., Hill, D. P., Massin, F., Farrell, J., Smith, R. B., & Taira, T. (2013). A fluid-driven earthquake swarm on the margin of the Yellowstone caldera. *Journal of Geophysical Research: Solid Earth*, 118(9), 4872–4886. DOI: [10.1002/jgrb.50362](https://doi.org/10.1002/jgrb.50362)

590

Shi, Z., Wang, G., Manga, M., & Wang, C.-Y. (2015). Mechanism of co-seismic water level change following four great earthquakes—Insights from co-seismic responses throughout the Chinese mainland. *Earth and Planetary Science Letters*, 430, 66–74. DOI: [10.1016/j.epsl.2015.08.012](https://doi.org/10.1016/j.epsl.2015.08.012)

- 595 Snieder, R., & Larose, E. (2013). Extracting earth's elastic wave response from noise measurements. *Annual Review of Earth and Planetary Sciences*, 41(1), 183–206. DOI: [10.1146/annurev-earth-050212-123936](https://doi.org/10.1146/annurev-earth-050212-123936)
- Steinberg, G. S., Merzhanov, A. G., & Steinberg, A. S. (1982). Geyser process: Its theory, modeling, and field experiment. Part 4. On seismic influence on geyser regime. *Modern Geology*, 8, 79–86.
- 600 Taira, T., & Brenguier, F. (2016). Response of hydrothermal system to stress transients at Lassen Volcanic Center, California, inferred from seismic interferometry with ambient noise. *Earth, Planets and Space*, 68(1), 162. DOI: [10.1186/s40623-016-0538-6](https://doi.org/10.1186/s40623-016-0538-6)
- 605 Taira, T., Nayak, A., Brenguier, F., & Manga, M. (2018). Monitoring reservoir response to earthquakes and fluid extraction, Salton Sea geothermal field, California. *Science Advances*, 4(1), e1701536. DOI: [10.1126/sciadv.1701536](https://doi.org/10.1126/sciadv.1701536)
- Teshima, N., Toramaru, A., & Ichihara, M. (2022). Precursory pressure oscillation in a laboratory geyser system. *Journal of Volcanology and Geothermal Research*, 429, 107613. DOI: [10.1016/j.jvolgeores.2022.107613](https://doi.org/10.1016/j.jvolgeores.2022.107613)
- 610 University of Utah Seismograph Stations. (2022). *M 3.9—22 km SSW of Mammoth, Wyoming* [dataset]. Advanced National Seismic System Comprehensive Catalog. URL: <https://earthquake.usgs.gov/earthquakes/eventpage/uu60515582/origin/detail>
- 615 Vandemeulebrouck, J., Sohn, R. A., Rudolph, M. L., Hurwitz, S., Manga, M., Johnston, M. J. S., Soule, S. A., McPhee, D., Glen, J. M. G., Karlstrom, L., & Murphy, F. (2014). Eruptions at Lone Star geyser, Yellowstone National Park, USA: 2. Constraints on subsurface dynamics. *Journal of Geophysical Research: Solid Earth*, 119(12), 8688–8707. DOI: [10.1002/2014JB011526](https://doi.org/10.1002/2014JB011526)
- 620 van der Elst, N. J., & Brodsky, E. E. (2010). Connecting near-field and far-field earthquake triggering to dynamic strain. *Journal of Geophysical Research*, 115, B07311. DOI: [10.1029/2009JB006681](https://doi.org/10.1029/2009JB006681)

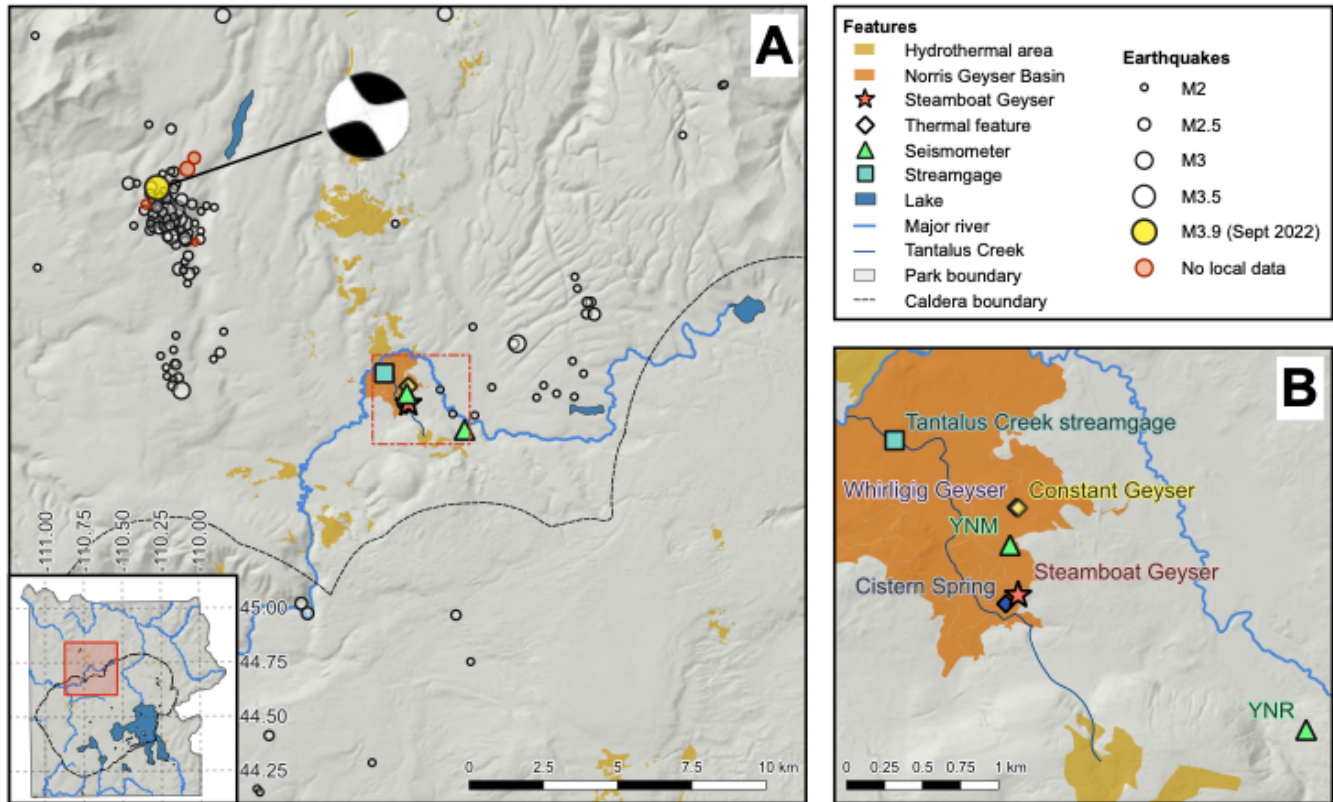
- 625 Waite, G. P., & Smith, R. B. (2002). Seismic evidence for fluid migration accompanying subsidence of the
Yellowstone caldera. *Journal of Geophysical Research: Solid Earth*, 107(B9), ESE 1. DOI:
[10.1029/2001JB000586](https://doi.org/10.1029/2001JB000586)
- 630 Walter, T. R., Wang, R., Zimmer, M., Grosser, H., Lühr, B., & Ratdomopurbo, A. (2007). Volcanic activity
influenced by tectonic earthquakes: Static and dynamic stress triggering at Mt. Merapi. *Geophysical Research
Letters*, 34(5). DOI: [10.1029/2006GL028710](https://doi.org/10.1029/2006GL028710)
- Wang, C.-Y., & Manga, M. (2015). New streams and springs after the 2014 Mw6.0 South Napa earthquake. *Nature
Communications*, 6, 7597. DOI: [10.1038/ncomms8597](https://doi.org/10.1038/ncomms8597)
- 635 White, D. E., Hutchinson, R. A., & Keith, T. E. C. (1988). *The geology and remarkable thermal activity of Norris
Geyser Basin, Yellowstone National Park, Wyoming* (Professional Paper 1456). U.S. Geological Survey. URL:
<http://pubs.usgs.gov/pp/1456/>
- Wolf, M. (2022). *Note ID 23890* [database entry]. Geysertimes. URL: <https://geysertimes.org/note.php?id=23890>
- 640 Wu, S.-M., Lin, F.-C., Farrell, J., & Allam, A. (2019). Imaging the deep subsurface plumbing of Old Faithful
Geyser from low-frequency hydrothermal tremor migration. *Geophysical Research Letters*, 46(13), 7315–7322.
DOI: [10.1029/2018GL081771](https://doi.org/10.1029/2018GL081771)
- 645 Wu, S.-M., Lin, F.-C., Farrell, J., Keller, W. E., White, E. B., & Hungerford, J. D. G. (2021). Imaging the subsurface
plumbing complex of Steamboat Geyser and Cistern Spring with hydrothermal tremor migration using seismic
interferometry. *Journal of Geophysical Research: Solid Earth*, 126(4), e2020JB021128. DOI:
[10.1029/2020JB021128](https://doi.org/10.1029/2020JB021128)
- 650 Yellowstone Volcano Observatory. (2023). *Yellowstone Volcano Observatory 2022 Annual Report* (Circular 1508).
U.S. Geological Survey. DOI: [10.3133/cir1508](https://doi.org/10.3133/cir1508)
- Zhong, S., Wan, Z., Duan, B., Liu, D., & Luo, B. (2019). Do earthquakes trigger mud volcanoes? A case study

This is an EarthArXiv **preprint** that has been submitted to *Volcanica*. It has **not yet** undergone peer review.

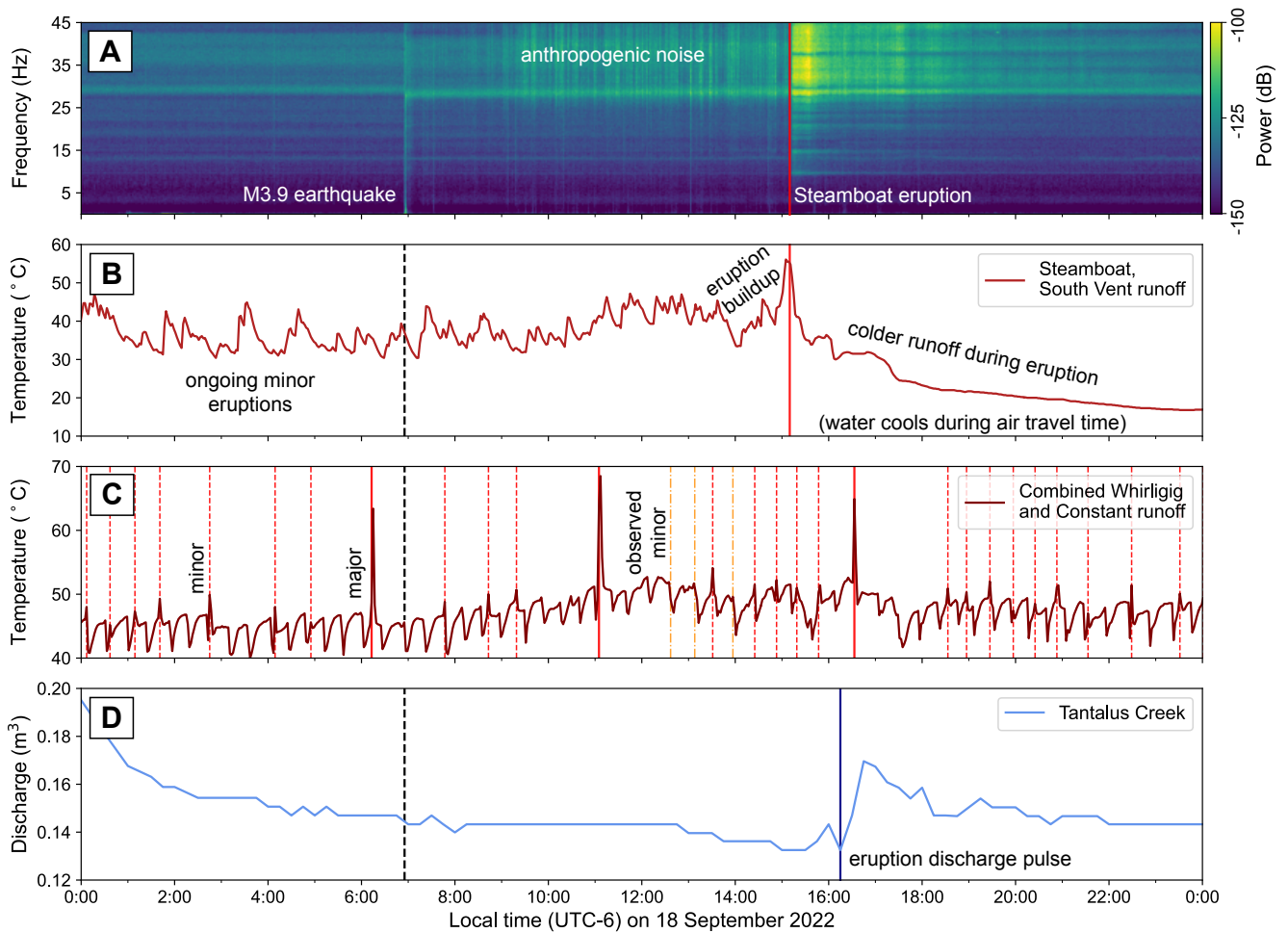
from the southern margin of the Junggar Basin, NW China. *Geological Journal*, 54(3), 1223–1237. DOI:

655 [10.1002/gj.3222](https://doi.org/10.1002/gj.3222)

Figures



660



665

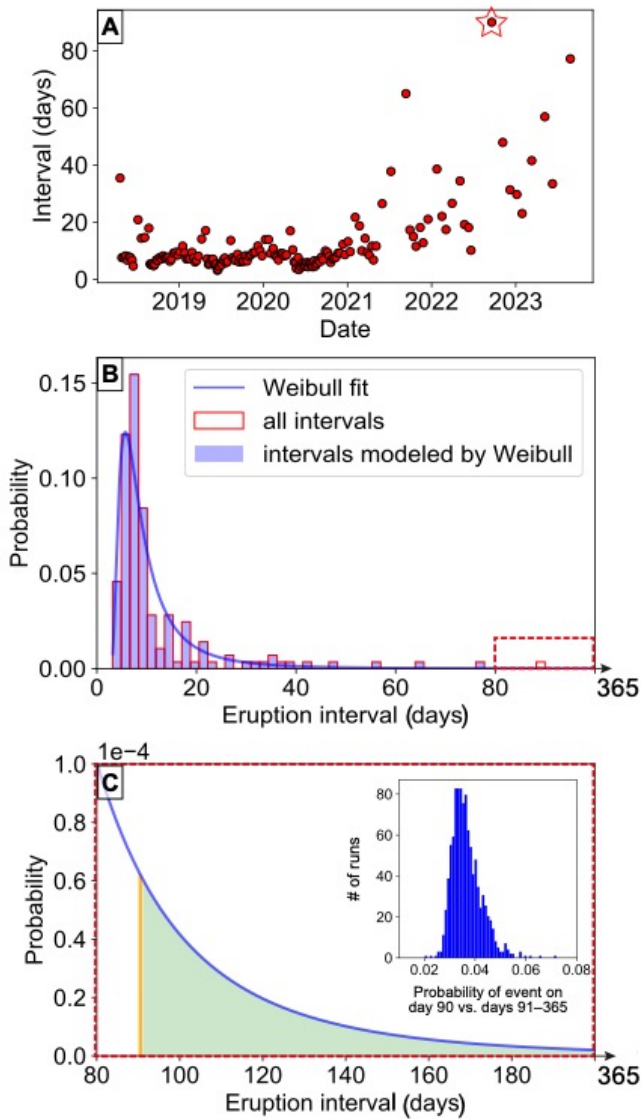
670

Figure 2: A visual summary of monitored thermal activity on 18 September 2022. In panels B–D, the earthquake timing is marked with a black dashed line. [A] Spectrogram of YNM vertical velocity data; power is clipped to the upper (-100 dB) and lower (-150 dB) bounds. [B] Temperature data from Steamboat’s South Vent runoff channel. The temperature drops during the eruption because most water first discharges through the jet and cools while traveling through the air. [C] Temperature data from a combined runoff channel for Whirligig and Constant. Red lines mark major (solid) and minor (dashed) eruptions in the GeyserTimes database. Gold dash-dotted lines indicate visual observations of a minor eruption without a corresponding E time entry. The short period oscillations are due to water level cycling in Constant Geyser between eruptions (which themselves are not detectable during this time period). [D] Hot spring and geyser discharge through Tantalus Creek.

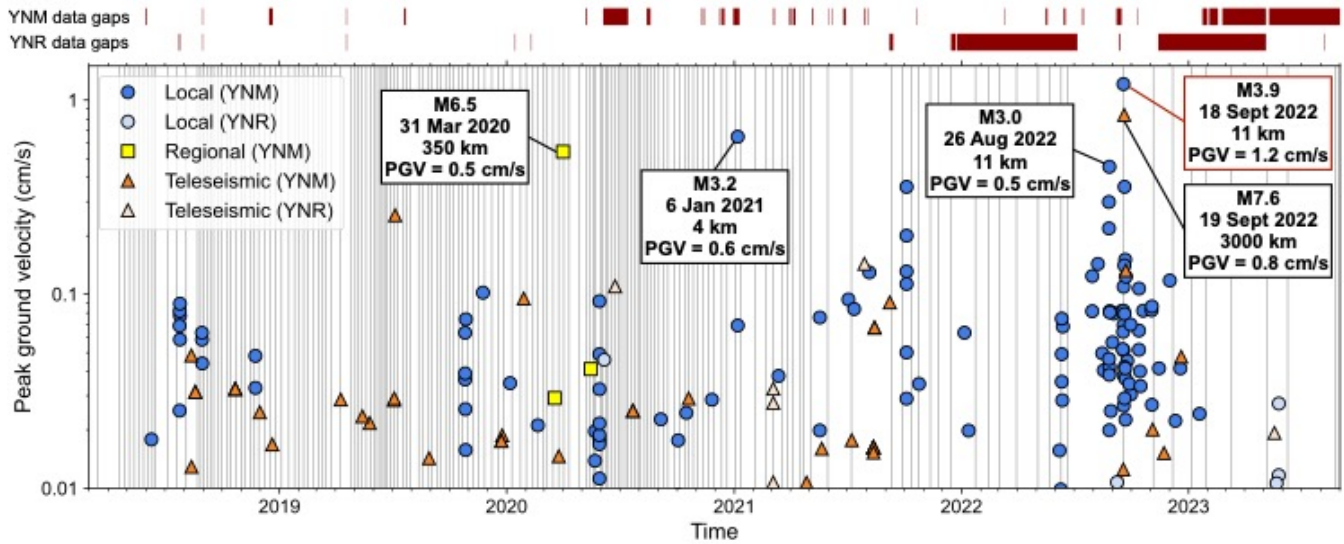


675

Figure 3: Steamboat Geyser in steam phase on 18 September 2022 at 17:58 local time (2.8 h after eruption initiation). Photo by Graham Meech.

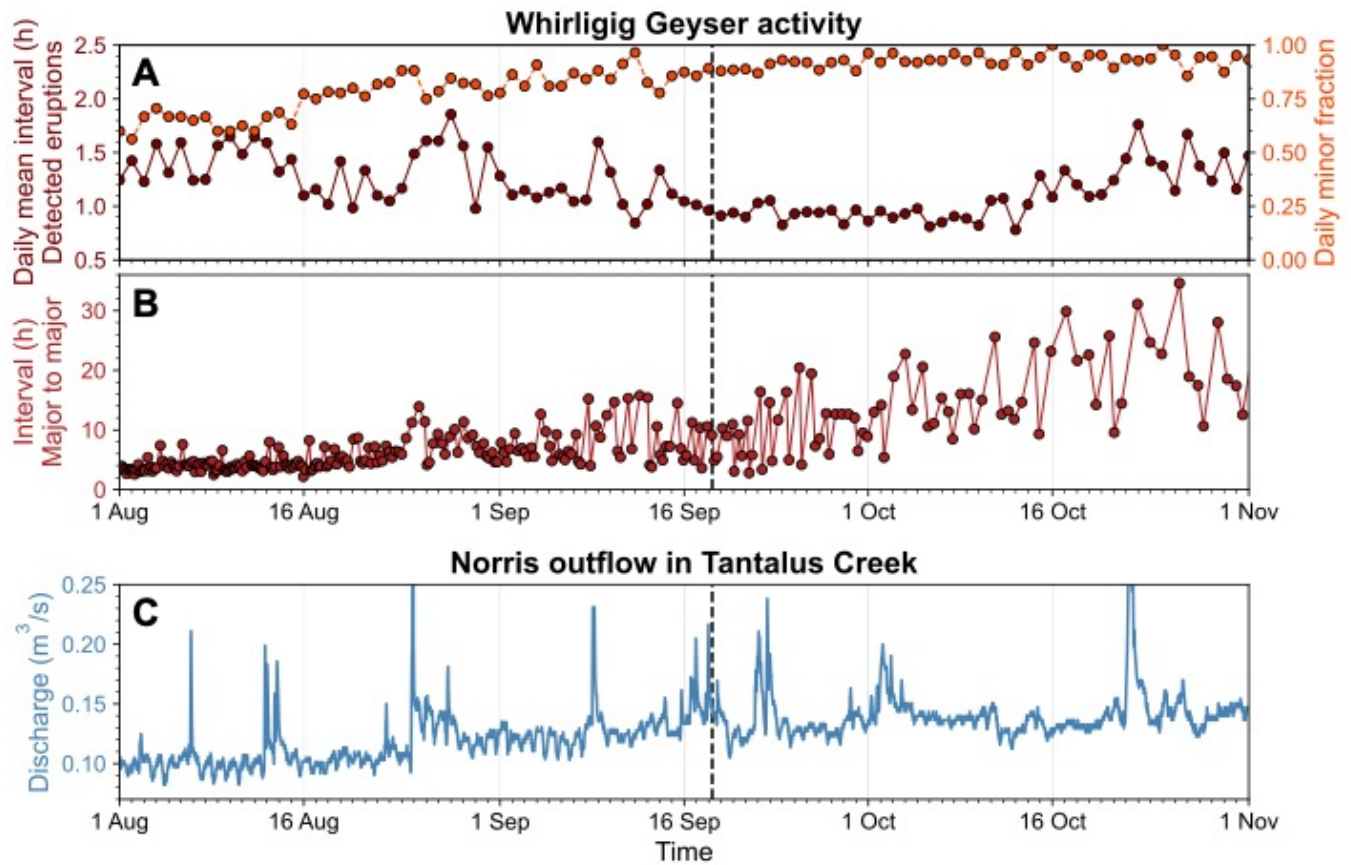


680 **Figure 4: [A] Interval between Steamboat's eruptions over time. The 18 September 2022 eruption is marked by a red star. [B] Probability density function for the Weibull fit (blue line) overlaid on discrete interval probabilities (the 90 d, post-earthquake eruption interval is not modeled). [C] Zoomed-in view of red, dashed box in [B]. We calculate the probability of eruption by dividing the area under the distribution for the day that it occurred (orange bar, day 90) divided by the area under the curve from days 91–365 (green shading). Inset histogram shows the results of following the same procedure for 1000 resamplings of the interval distribution.**



685

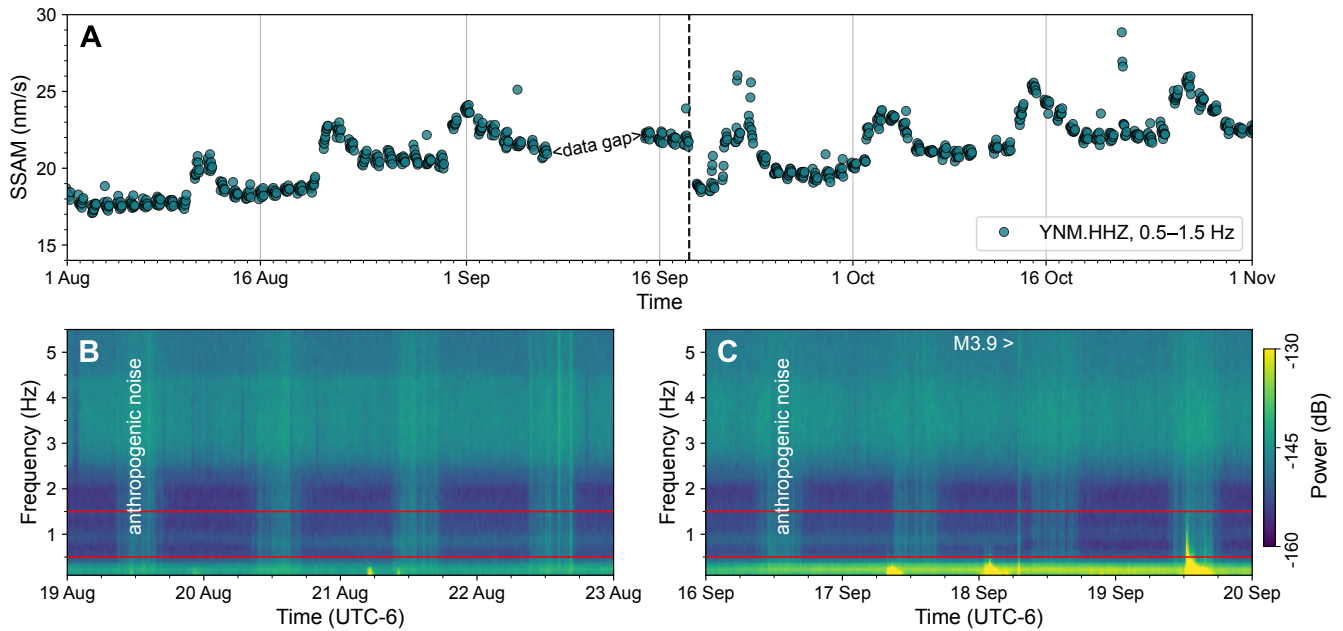
Figure 5: PGV associated with local, regional (<1000 km), and teleseismic earthquakes between March 2018 and September 2023. YNR data (lighter colors) are shown when YNM was offline or noisy. Gray vertical lines mark Steamboat eruptions and dark red boxes above the plot show data gaps for the two broadband stations. We label five events including the M3.9 earthquake (red box) with their magnitude, date, distance from Steamboat, and PGV.



690

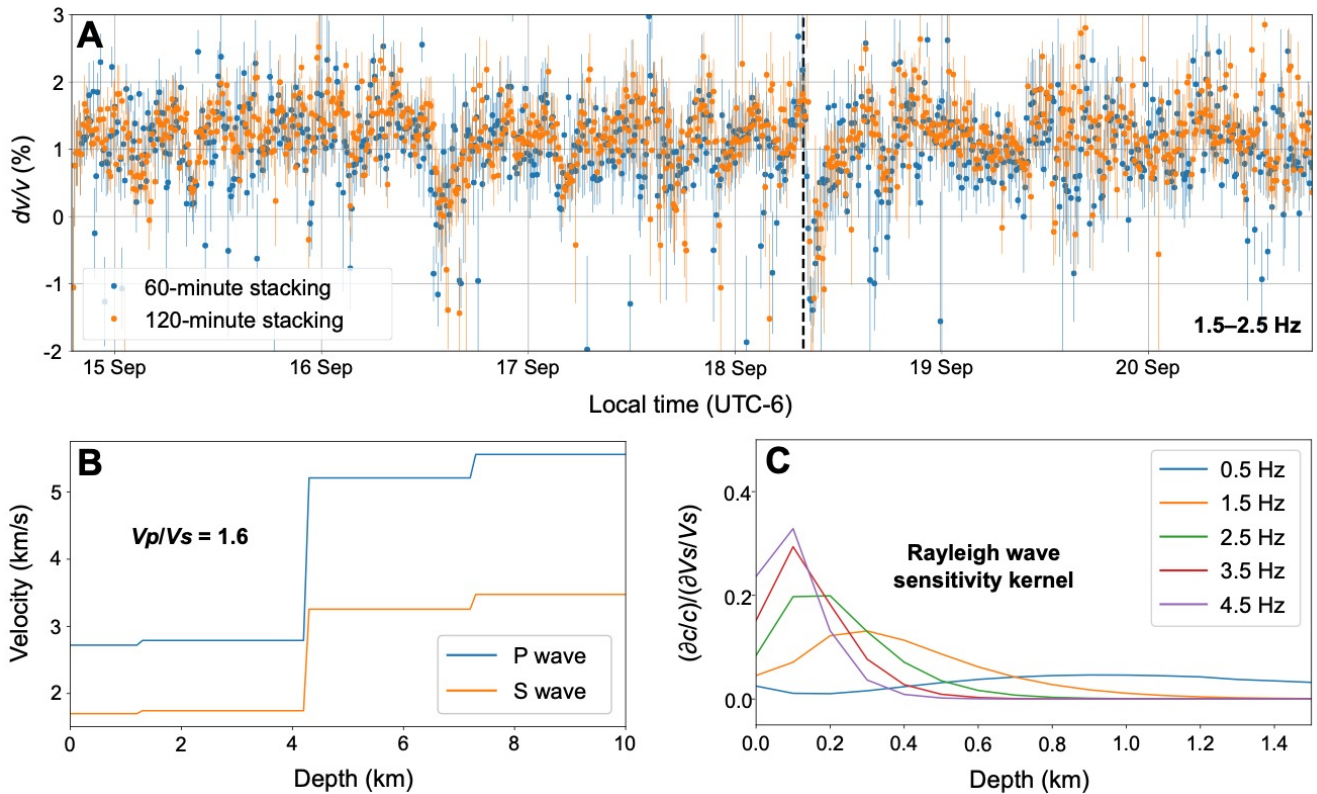
Figure 6: Summary of continuous surface hydrothermal data considered in Section 5.1. The black vertical line in each panel marks the time of the M3.9 earthquake. [A] Daily mean interval for Whirligig Geyser eruptions detected by the YVO temperature logger (dark red). We also show the fraction of minor eruptions occurring each day (orange). [B] Intervals between major Whirligig eruptions. [C] Discharge in Tantalus Creek. All discharge spikes occur due to rainfall events except for the pulse from Steamboat's eruption on 18 September.

695



700

Figure 7: SSAM and spectrograms related to vertical velocity data at station YNM. [A] Overnight SSAM for 1 h segments in the 0.5–1.5 Hz band during August–October 2022. There is a step change after the M3.9 earthquake (black dashed line). [B] Spectrogram for 19–23 August (blue dashed box in [A]). The periodic SSAM signal is related to a small decrease in peak frequency and slight increase in power between 0.5–2.0 Hz. [C] Spectrogram of 16–20 September (green dashed box in [A]). After the earthquake, there is a small increase in peak frequency and a subtle decrease in power between 0.7–2.2 Hz. The three low-frequency signals are due to teleseismic earthquakes. Spectrograms in [B] and [C] show power clipped to -160 and -130 dB and red lines encapsulate the 0.5–1.5 Hz band.



705 **Figure 8: [A]** Relative velocity changes (dv/v) with error bars extending to ± 2 standard deviations for a frequency
 band of 1.5–2.5 Hz in the days around the M3.9 earthquake (dashed black line). Both 60 min (blue) and 120 min
 (orange) stacking methods show a decrease in dv/v immediately following the earthquake. The second largest PGV
 (0.8 cm/s) during the active phase occurs on 19 September just before 12:23 without a corresponding decrease in
 dv/v . **[B]** Velocity model assuming v_p/v_s is 1.6 (Husen et al. 2004). **[C]** Sensitivity kernel calculated from the velocity
 710 model in [B], assuming the coda of NCFs is dominated by Rayleigh waves. Because the decrease in dv/v appears only
 in the 1.5–2.5 Hz results, we infer the change most likely occurred at 300–500 m depth where the sensitivity to 1.5–
 2.5 Hz is highest relative to the other frequencies.